6-1990

A Numerical Study of the Interaction Between a Deep Cold Jet and the Bottom Boundary Layer of the Ocean

Tal Ezer
Old Dominion University, tezer@odu.edu

Georges L. Weatherly

Original Publication Citation

Ezer, T., & Weatherly, G.L. (1990). A numerical study of the interaction between a deep cold jet and the bottom boundary layer of the ocean. *Journal of Physical Oceanography, 20*(6), 801-816. doi: doi:10.1175/1520-0485(1990)0202.0.CO;2

A Numerical Study of the Interaction between a Deep Cold Jet and the Bottom Boundary Layer of the Ocean

TAL EZER* AND GEORGES L. WEATHERLY*

Department of Oceanography, Florida State University, Tallahassee, Florida

(Manuscript received 1 May 1989, in final form 21 August 1989)

ABSTRACT

A two-dimensional (x–z) primitive equation model is used to study the interaction between a deep cold jet on a sloping bottom and the bottom boundary layer (BBL) of the deep ocean. Two closure schemes are used: a standard second order turbulence closure (SOTC) scheme (the level 2½ model of Mellor and Yamada), and a new eddy viscosity closure scheme (K-model). The latter is a computationally simple model that produces very similar eddy viscosity and velocity fields as the more complicated SOTC-model while saving about 20% of the computational time.

The results of the numerical simulations compare favorably to observations from the base of the North Atlantic continental rise where the cold jet known as the Cold Filament (CF) is found. The interaction between the CF and the BBL is found to be dominated by cross-isotherm Ekman flow, resulting in an asymmetry effect with different dynamics at each one of the fronts associated with the CF. Some of the unusual characteristics of this region are explained with the aid of the numerical experiments. These are: velocity profiles significantly different from those obtained by classical Ekman dynamics, unstable BBLs and detachment of bottom layers. Spatial variations in the characteristics of the BBL which are often neglected in deep-ocean studies are found to be significant in this region.

1. Introduction

Pools or ribbons of cold water flowing on the bottom of the ocean are not uncommon features in the western North Atlantic (e.g., Armi and D'Asaro 1980; Ebbesmeyer et al. 1986; Weatherly and Kelley 1982). In this paper, the dynamics of one such a feature, the Cold Filament (CF) (Weatherly and Kelley 1982, 1985) is studied with a numerical model.

In previous analytical studies of cold eddies on a sloping bottom (e.g., Nof 1983) or cold stream bottom flow (e.g., Smith 1975), bottom friction was either neglected (the former one) or was taken in a form of a simple drag law (the latter one). External forcing is often neglected as well in such studies. However, in the energetic region discussed here [i.e., in the High Energetic Bottom Boundary Layer Experiment (HEBBLE) area, at ~40°N, 63°W, ~4900 in depth], bottom turbulence and boundary layer dynamics may play a dominant role. The complicated interaction between a CF-like feature and the BBL suggests that numerical rather than analytical models are preferred to study this region. On the other hand, numerical models used to study the deep-ocean BBL are often one-dimensional (e.g., McLean and Yean 1987; Richards 1982; Weatherly and Martin 1978), assuming negligible spatial variations. However, in the HEBBLE area the near-bottom layers show significant spatial variations with frontal structures having horizontal scales of a few internal Rossby radii of deformation for the CF (Ezer and Weatherly 1989a).

Notwithstanding the observations of Weatherly and Kelley (1982, 1985) that suggest that the CF is a relatively stable, robust feature, the study of Griffiths et al. (1982) could be interpreted to imply that a CF-like feature would be unstable and would break up. However, there are some reasons to believe that this inference may not be appropriate for the CF case. First, breakup of a jet into a chain of eddies in their study occurred only when the width of the jet was comparable to its radius of deformation, while the CF width is more than eight times its radius of deformation. Second, the jets considered by them were essentially frictionless, while the CF is highly frictional flow.

The simple linear BBL model of Ezer and Weatherly (1989) indicates the spatial variations of the BBL and the bottom mixed layer (BML) thicknesses and the distinction between the two across the CF. Nevertheless, nonlinearity in the momentum equations, temperature advection and horizontal diffusion effects may

* Also affiliated with Geophysical Fluid Dynamics Institute, Florida State University, Tallahassee, Florida.

Corresponding author address: Dr. Tal Ezer, Program in Atmospheric and Oceanic Sciences, Princeton University, P.O. Box 308, Princeton, NJ 08542.

be important in the frontal dynamics. Thus a more complicated two-dimensional (x–z) primitive equation BBL model is used in the present study. This model is a modified version of the thin-shell BBL submodel of the Sandia Ocean Modeling System (Dietrich et al. 1987) developed at Sandia National Laboratories and at Florida State University.

Two different approaches that are often used in modeling of a turbulent regime are presented here: a second order turbulence closure scheme (SOTC-model), and an eddy viscosity closure scheme (K-model). The first one is the Mellor and Yamada (1974, 1982) level 2½ scheme. It requires solving numerically the time-dependent turbulent kinetic energy (TKE) equation to formulate the eddy coefficients. The second one uses the eddy diffusivities expressions of Ezer and Weatherly (1989) together with a new formulation for unstable regions; it parameterizes the eddy coefficients directly from the flow and the temperature fields thus it is more efficient than the first one. In a CF or a cold eddy, the BML is not the sole result of bottom mixing and thus the parameterization of the eddy diffusivity depends on the imposed scale of the feature (Ezer and Weatherly 1989). However, such formulations can predict reasonable eddy diffusivity only in cases of stable or neutral stratifications where the turbulence is produced by bottom friction. In the case discussed here however, it is found that cross isotherm flow may result in unstably stratified regions. In this case, where turbulence is produced by thermal convection, an entirely different parameterization is needed. By assuming the appropriate physical balance in the TKE equation, and neglecting shear turbulence, a new formulation for thermal turbulence, which agrees with the results of the SOTC-model, is suggested. To eliminate possible confusion, the semantics used throughout this paper are as follows: a stably stratified case is one that has a homogeneous potential temperature in the BML with stable transition layer above it; a neutrally stratified case is one that has potential temperature homogeneous everywhere; an unstably stratified case is one that has an unstable region somewhere in the water column.

The general goal of this study, is to investigate the two-way interaction between the CF and the BBL, i.e., to answer the following questions: (i) how does the BBL dynamics affect the structure of the CF? and (ii) how does the existence of the CF modify the dynamics of the BBL? The motivation for such a study comes from BBL observations in this region which indicate some unusual phenomena there, such as occasional unstably stratified BBL's, velocity profiles which are much different than those obtained by classical Ekman dynamics, and detached bottom layers (Weatherly and Kelley 1985). It is hypothesized that these characteristics are related to the existence of the CF in this area. As a first step in such a preliminary study, only a two-dimensional (x–z) case with constant along-slope flow is considered. Since a constant flow can be found up to periods of the order of about two weeks (Kelley et al. 1982), primarily short term simulations are presented here.

2. The model equations and the closure schemes

a. The model equations

A two-dimensional (i.e., no variations in the y-direction) case with constant slope in the x-direction is assumed. A coordinate system that follows the bottom $Z_B = -sx$ is used (i.e., z is the distance from the bottom and x pointed downslope). Since the bottom slope is assumed to be very small ($s = 0.005$ in the study area) the transformation of the velocity components into ones in a vertical coordinate system (indicated by superscript v) is $v^v = v$, $u^v \approx u$ and $w^v \approx w - su$. An incompressible fluid with hydrostatic, turbulent (i.e., large Reynolds numbers) flow on an f-plane is assumed. Thus the momentum, heat and continuity equations can be written as

$$u_t - f(v - V_g) + uu_x + wu_z = (A^x u_x)_x + (K_M u_z)_z \quad (1a)$$

$$v_t + fu + uv_x + wv_z = (A^y v_x)_x + (K_M v_z)_z \quad (1b)$$

$$\theta_t + u\theta_x + w\theta_z = (A^x \theta_x)_x + (K_H \theta_z)_z \quad (1c)$$

$$u_x + w_z = 0 \quad (1d)$$

with lower case subscripts x, z, t indicating partial derivatives. The eddy coefficients for transfer of momentum and heat in the vertical K_M and K_H, and the horizontal eddy coefficients A^x and A^y are defined later. With the linear equation of state approximation the geostrophic component can be estimated from the potential temperature (θ) field,

$$V_g(x, z, t) = V_0 - (\beta g/f) \int_z^{H_T} \theta_x dz - (s\beta g/f)(\theta_1 - \theta) \quad (2)$$

where $\beta = 9.4 \times 10^{-5}$ °C^{-1} is the coefficient of thermal expansion chosen to give realistic density structure, g is the gravitational acceleration, $\theta_1 = 1.83$°C and $V_0 = -0.1$ m s^{-1} are the potential temperature and the velocity of the interior on the top of the modeled area at $z = H_T = 200$ m. The second term on the right-hand side of (2) represents pressure gradient-driven velocity (the thermal wind effects that are discussed later derive from this term). The third term which sometimes is added directly to the momentum equations (e.g., Weatherly and Martin 1978) represents "buoyant-slope" effect and is the term which gives the translation component of cold eddies on a sloping bottom (Nof 1983).

b. The horizontal diffusion coefficients

Following Yamada (1979), for a two-dimensional flow, the eddy coefficients for horizontal diffusion may be taken in the form $A^x = 0.02(\delta x)(\delta y)|u_x|$ and $A^y = 0.01(\delta x)(\delta y)|v_x|$ where δx and δy are the numerical grid spacing in the x and y directions, respectively. The two-dimensional nature of our case implies that $\delta y \gg \delta x$, and for $\delta y = 50\delta x$,

$$(A^x, A^y) = (\delta x)^2|u_x, 0.5v_x|. \tag{3}$$

The choice of the ratio $\delta x/\delta y$, which represents an approximated ratio between the corresponding scales of the CF, is supported by dimensional argument: in a frontal region where only variations in the x direction are allowed, (1c) implies that $A^x \approx u(\delta z) \approx (\delta x)^2 u_x$. For our case the resulting horizontal eddy coefficients are 1–10 $m^2\ s^{-1}$ near the frontal regions. Note that these values are smaller by about one order of magnitude than the values approximated by $A^x = \langle u'^2 \rangle T_0$ and $A^y = \langle v'^2 \rangle T_0$ (Boning 1988) for representative variances, $\langle u'^2 \rangle$, $\langle v'^2 \rangle$ and integral time scale, T_0 of this area. However, the validity of the former relations is doubtful in energetic regions with strong shear (Boning 1988) such as the HEBBLE area. Moreover, the large variability of the HEBBLE area results from energetic fluctuations in the mesoscale eddies range (Kelley and Weatherly 1985); thus for our short-term, constant forcing case it may be inappropriate to use long-term variance values to approximate local horizontal diffusivity. Note that since $u/v \approx 0.1$, $A^y \approx 5A^x$.

c. Second-order turbulence closure scheme

The SOTC-model used here is the Mellor and Yamada (1974, 1982) level-2½ scheme in the form used by Yamada (1979). The equation for the TKE, $E = \frac{1}{2}q^2$ where $q = (u'^2 + v'^2 + w'^2)^{1/2}$ is the fluctuating velocity magnitude, is written as

$$E_t + uE_x + wE_z = (A^x E_x)_x + (K_E E_z)_z + K_M(u_z^2 + v_z^2) - K_H \beta g \theta_z - q^3/Cl \tag{4}$$

where $K_E = 0.2ql$ and $C = 16.6$ is an empirical constant. The terms on the right-hand side of (4) represent the horizontal and vertical diffusion, shear and buoyant production, and dissipation of TKE. The length scale l is calculated by

$$l = kz(1 + kz/l_0)^{-1} \tag{5a}$$

$$l_0 = \tau \int_0^{H_T} zq dz \Big/ \int_0^{H_T} q dz \tag{5b}$$

where $k = 0.4$ is the von Kármán parameter, and $\tau = 0.2$ is a length scale factor (Mofjeld and Lavelle, 1984). For this closure scheme the eddy coefficients for vertical diffusion of momentum and heat, K_M and K_H, are

$$K_M = \frac{A_1 l q^3 (R_1 q^2 + R_2 l^2 T^z)}{q^2(q^2 + R_3 l^2 V^z) + R_4 l^2 T^z (R_5 l^2 V^z + R_6 q^2 + R_7 l^2 T^z)} \tag{6a}$$

$$K_H = \frac{A_2 l (q^3 - R_8 l K_M V^z)}{q^2 + R_9 l^2 T^z} \tag{6b}$$

(Yamada 1979) where $T^z = \beta g \theta_z$, $V^z = u_z^2 + v_z^2$ and the empirical constants are $(A_1, A_2, R_1, R_2, R_3, R_4, R_5, R_6, R_7, R_8, R_9) = (0.92, 0.74, 0.76, 10.15, 5.08, 2.09, 43.5, 17.98, 91.8, 5.52, 30.6)$. In this kind of formulation, the eddy coefficients at each point depend on the local turbulence, q, on the length scale, l, on the local stratification parameter, T^z, and on the vertical shear parameter, V^z.

d. K-model for bottom turbulence

An alternative to the SOTC-model is the so called K-model in which the eddy coefficients are calculated directly from the velocity field and the stratification without solving the TKE equation. However, for a region where a cold eddy or the CF are found, the parameterizations of the eddy coefficients are more complicated than the ones often used in models of the oceanic or the planetary boundary layer (for example, see Arya 1973, for a comparison between some of the commonly used K-models) since the imposed scale of the cold feature should be taken into account (Ezer and Weatherly 1989). In a region of neutral or stable stratification with BML thickness H, where bottom friction is the main source of turbulence, the eddy coefficients are taken as

$$K_M = ku_* z\left[1 - \frac{(z - Z_{\max})^2}{(H - Z_{\max})^2}\right] \exp[-z/Z_{\max}) \qquad 0 < z < H \tag{7a}$$

$$K_H = A_0 K_M \tag{7b}$$

(Ezer and Weatherly 1989). The friction velocity, u_* is approximated by $0.035|V_g|$, and the mixed layer depth $H(x, t)$ is specified from the temperature profile at each x. $K_0 = 10^{-4}\ m^2\ s^{-1}$ is chosen to represent the background turbulence in the interior (at $z \geq H$) (this is the value suggested by Munk 1966). To ensure the continuity of K_M in the upper portion of the BML, K_M is set to K_0 if (7a) gives a value smaller than K_0. The ratio between the eddy coefficients $A_0 = 1.3$ is chosen. This value represents fairly well the value calculated by (6) for our conditions and is also close to the ratio given by different models and observations for neutral stratification (Yamada 1975). Here $Z_{\max}$ is the height where K_M is maximum and is given by

$$Z_{\max} = 1.7[L_0(2 + H/h_{\max}) + L_1(1 - H/h_{\max})] \tag{8}$$

for $H < h_{max}$ (Ezer and Weatherly 1989) where $L_0 = u_*^2(V_g f)^{-1}$ and $L_1 = 1$ m are length scales, and $h_{max} = 1.3(u_*/f)$ is the BBL thickness in neutral stratification. For neutral stratification or when $H > h_{max}$ (8) reduces to $Z_{max} \approx 0.16(u_*/f)$ which is the value suggested by other models (e.g., Mofjeld and Lavelle 1984). The above formulation predicts K_M values very similar to those calculated by the Mellor and Yamada level 2½ scheme (i.e., section 2h).

The details of the formulation of the eddy coefficients and the resultant K_M profiles for different conditions are given in Ezer and Weatherly (1989). However, for the completeness of this paper, some of the characteristics of the above formulations are described below: K_M increases linearly with distance from the bottom in the logarithmic layer, reaches a maximum value at height Z_{max}, and decreases to a small value K_0 at the top of the BBL. The height where $K_M = K_0$ is either the top of the BML, H for thin BMLs, or h_{max} for too thick BML (i.e., if $H > h_{max}$ the BBL is identical to the neutrally stratified case). In contrast to some K-models used in the stably stratified atmospheric boundary layer (e.g., Businger and Arya 1974) where K_M depends directly on the stratification, in the current scheme the stratification is implemented in the above formulas through the thickness of the BML. The thickness of the BML may be calculated by a numerical model, or from the stratification of the interior by empirical formulas such as the one suggested by Weatherly and Martin (1978). The advantage of the current scheme is its ability to deal with the special BMLs associated with cold eddies or filaments, in addition to the "classical" BBLs (i.e., those formed by bottom friction mixing the stratified interior). However, compared to the SOTC-models, the K-model can apply only to cases where the BML is well defined.

e. K-model for thermal turbulence

The results of the numerical model, as well as observations, show that in some regions an unstable stratification may exist due to cross-isotherm advection in the BBL (this will be discussed in detail in the following sections). Therefore, a formulation of the eddy coefficient in the form of (7) is insufficient when thermal instability rather than vertical shear is the major source of turbulence in such regions. For shear turbulence the basic balance in the TKE equation [Eq. (4)] is between the shear production and the dissipation terms. However, for thermal turbulence the basic balance is between the buoyant production and the dissipation terms, namely

$$q^3/Cl = -K_H \beta g \theta_z \tag{9}$$

(Tennekes and Lumley 1972). Assuming $\theta_z < 0$ and $V^z = 0$, (6) become

$$K_M = \frac{A_1 l q^3 (R_1 q^2 + R_2 l^2 \beta g \theta_z)}{q^4 + R_4 l^2 \beta g \theta_z (R_6 q^2 + R_7 l^2 \beta g \theta_z)} \tag{10a}$$

$$K_H = \frac{A_2 l q^3}{(q^2 + R_9 l^2 \beta g \theta_z)}. \tag{10b}$$

Eliminating q and K_H from (9) and (10b) and substituting q into (10a) gives the following formulas for the eddy coefficients and the fluctuating velocity magnitude:

$$K_m = C_1 l^2 (-\beta g \theta_z)^{1/2} \tag{11a}$$

$$K_H = C_2 l^2 (-\beta g \theta_z)^{1/2} \tag{11b}$$

$$q = C_3 l (-\beta g \theta_z)^{1/2} \tag{11c}$$

where $(C_1, C_2, C_3) = (14.25, 16.93, 6.55)$. The length scale, l, is calculated by (5a) specifying $l_0 = \tau^2(u_*/f)$ (Mofjeld and Lavelle 1984). Although the use of eddy diffusivity in a convective region is not yet a well approved theory (Tennekes and Lumley 1972), (11) at least approximates the values calculated by the level 2½ scheme, which is widely used in numerical models of the ocean and the atmosphere. Equation (11b) is consistent with studies of the free convection in the atmosphere, where C_2 is replaced by h_p/k^2; h_p (the free convection parameter of Priestly) usually taken as 0.9, but can be as large as 2.5 for Richardson number of -0.002 (Priestly 1959). For the largest value of h_p, $h_p/k^2 = 15.6$ is comparable to C_2; otherwise it is somewhat smaller. As will be shown later, in unstable regions (11a) predicts an eddy viscosity field which is in good agreement with the one calculated by the SOTC-model.

While in the K-model (11) is used to add thermal turbulence in unstable regions, it can also be used to improve the performance of the SOTC-model in extreme unstable cases. In a numerical model solving the complete set (4) and (6) (i.e., the SOTC-model), (10b) indicates that for unstable stratification K_H may reach infinitely large or even negative values if $q^2 \leq |R_9 l^2 \beta g \theta_z|$. This may occur due to the averaging of the numerical scheme, too coarse a grid, or the inclusion of addition terms in Eq. (4). The common use of a small default value in such cases gives unphysical results and thus (11) may be used to improve SOTC-models.

f. The initial and the boundary conditions

The initial CF core thickness is specified as

$$H_I(x) = H_0[1 - (x/x_0)^2] \tag{12}$$

which is in a similar form to the cross section of a cold eddy with a linear orbital velocity profile (Nof 1984). The maximum thickness of the core is taken as $H_0 = 100$ m (Weatherly and Kelley 1982), and the radius

is taken as $x_0 = 5$ km (Ezer and Weatherly 1989a). The initial potential temperature is taken as

$$\theta(x, z) = \begin{cases} \theta_0, & z < H_I \\ \theta_1 - B \times \exp[(h_I - z)/l_1], & z \geqslant H_I \end{cases} \quad (13)$$

where $\theta_1 = 1.83$°C, $B = 0.05$, and $l_1 = 60$ m (Fig. 5a). The coefficients in (13) are chosen to fit the temperature gradients in the transition region above the BML as the ones reported by Weatherly and Kelley (1982). The forcing velocity increases from zero linearly with time in the first two days until it reaches its constant value of V_0. This helps to reduce inertial oscillations in the spinup period of the model. The initial eddy coefficients are specified by (7) with u_* approximated by $0.035|V_0|$.

Equations (1a)–(1c) [and Eq. (4) in the SOTC-model] are solved in the region $-X_0 < x < X_0$, $z_0 < z < H_T$ with $H_T = 200$ m and $X_0 = 20$ km. A roughness length, $z_0 = 1.6 \times 10^{-4}$ m, is chosen; this value represents the average roughness for this region (Gross et al. 1986). The following boundary conditions were applied. At the bottom there is the no-slip condition and no flux of heat and TKE; thus

$$u = v = w = E_z = \theta_z = 0, \quad \text{at} \quad z = z_0. \quad (14)$$

Near the bottom, a logarithmic velocity profile is assumed:

$$u(z) = (u_*/k) \ln(z/z_0). \quad (15)$$

Thus, the direction of the flow at the first level z_1 is the same as that at the second level z_2 and its amplitude is found by (15). This allows a larger time step in the numerical model since a very fine grid near the bottom is not needed. The only requirement is that z_2 is in the logarithmic region ($z_2 = 0.5$ m was chosen in our case). Experiments with different vertical grids show that choosing a finer grid would not change the results significantly. The details of the numerics involved in this boundary condition are described by Dietrich et al. (1987). The upper boundary conditions are specified at height $H_T > H$,

$$u_z = w_z = E_z = \theta_z = 0, \quad v = V_0, \text{ at } z = H_T. \quad (16)$$

Since the interior outside the studying area (i.e., at $X_0 < |x|$) is not assumed to be at rest but is affected by the same forcing as the CF itself, the velocity there cannot be specified; thus

$$u_x = v_x = E_z = \theta_x = 0, \quad \text{at} \quad x = \pm X_0. \quad (17)$$

Since the width of the CF is smaller compared to the total width of the model (i.e., $x_0 \ll X_0$), spatial variations far from the CF are neglected. (In some of the figures however, only a portion of the total simulated area is shown; Fig. 5 however represents the whole domain).

g. *The grid system and the numerical scheme*

A logarithmic-plus-linear vertical grid (as in Yamada 1979) is used. That is, the grid is approximately logarithmic near the bottom and linear at higher levels. The maximum δz (near the top of the model) is about 5 m. A staggered "C" grid is used with a horizontal grid of $\delta x = 250$ m so that the fronts, which have a horizontal scale of order 1 km, could be resolved.

The numerical schemes are described by Dietrich et al. (1987). However, there are several differences from Dietrich et al. (i) the horizontal eddy coefficients are calculated from velocity gradients rather than velocity amplitudes, (ii) the filtered version of the leapfrog scheme is not used thus horizontal diffusion and shear production of TKE terms are treated in a forward way such that each term is numerically stable by itself, (iii) thermal wind effects were added to the original version of the model (i.e., the geostrophic component is allowed to change inside the BBL due to the stratification).

The vertical velocity is calculated by integration of the continuity equation (1d).

The most restricted condition on the time step is $C\delta t/\delta x \ll 1$, where C is the phase velocity of the fastest internal wave. For the parameters used, a time step of $\delta t = 30$ min gave a stable numerical solution for runs of as long as tens of days without any nonlinear numerical instability.

The same numerical scheme is used for the K-models where the formulas in sections 2d and 2e are used instead of solving numerically the TKE equation.

h. *A comparison between the K-model and the SOTC-model*

In the SOTC-model the eddy kinetic energy is found by solving (4), the length scale is calculated by (5) and then the vertical eddy coefficients are found from (6). In the K-model the vertical eddy coefficients are calculated by (7), and in unstable regions (11a) and (11b) are used to add a thermal turbulence effect. The K-model is more efficient in that it requires fewer computations and less storage than the SOTC-model (for the two-dimensional model used here the K-model saves up to 20% of the computations). In the next section the results of the SOTC-model are discussed; here only the comparison between the two models is discussed.

The results show good agreement in the temperature fields (Fig. 1), the velocity fields (Fig. 2) and the vertical eddy coefficient fields (Fig. 3) calculated by the two models. The K-model produces a somewhat larger BBL thickness in the downslope side of the CF. This results

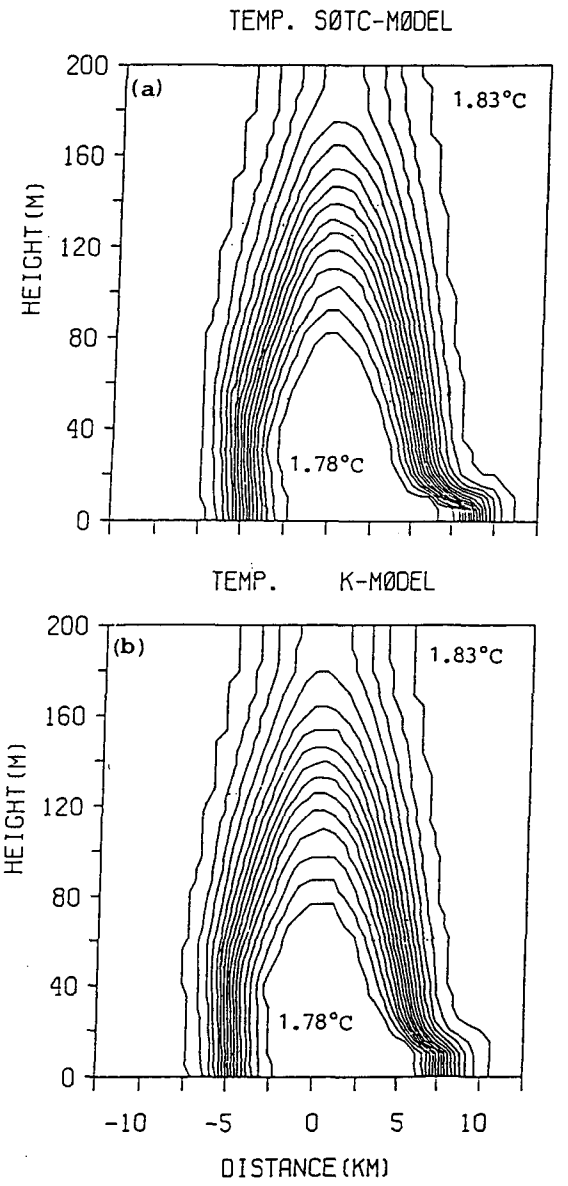

FIG. 1. The potential temperature structure of the CF (in bottom embedded coordinates) after 4 days of simulation with $V_0 = -0.1$ m s^{-1}. (a) Calculated by the SOTC-model. (b) Calculated by the K-model.

from the uncertainty in identifying the BML thickness from the temperature structure in the K-model (it is needed in the parameterization of the eddy diffusivity). However, generally the agreement between the two models is good in all stability regions (Fig. 4 shows the stability across the CF for the K-model, which is generally quite similar to the one obtained by the SOTC-model). A more detailed comparison may be done in the future; the major goal of the present study, however, is the physical interpretations of the numerical experiments.

3. A comparison between the numerical experiments and observations

a. The interaction between the BBL and the CF

The results of the SOTC-model will be discussed here in light of some observations of the BBL associated with the CF. (For the short-term simulations presented here, there is not much difference which scheme is used; however for future longer runs, the more economical K-model is advantageous). The comparison in this section has two purposes: 1) to check the ability of the numerical model to predict realistic bottom boundary

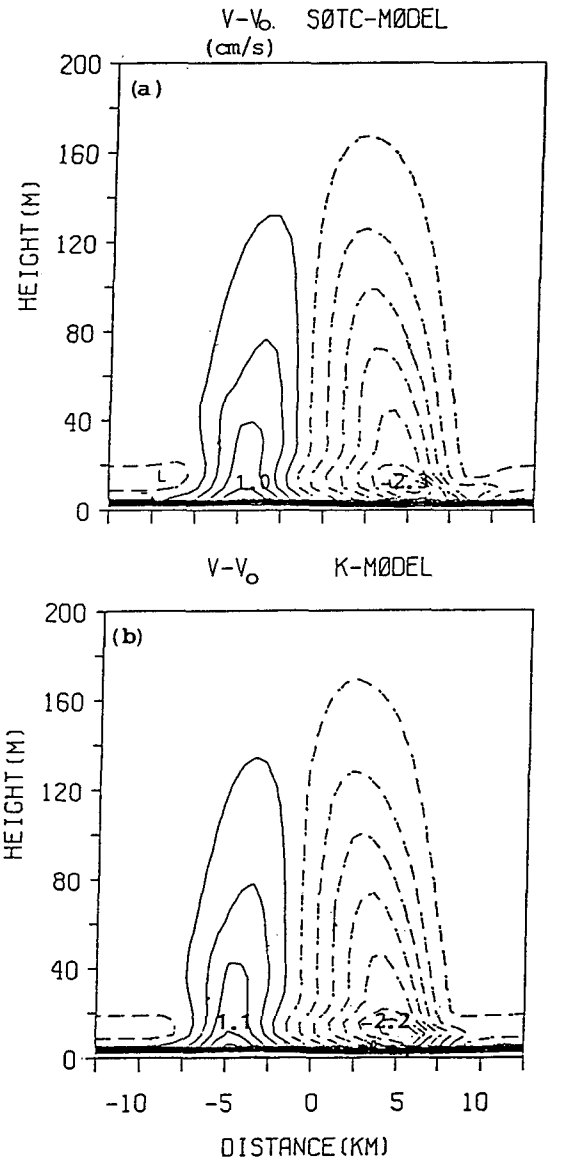

FIG. 2. As in Fig. 1, but for the along slope velocity component relative to the geostrophic velocity of the interior ($v - V_0$). Dashed lines represent absolute velocity greater than the interior velocity.

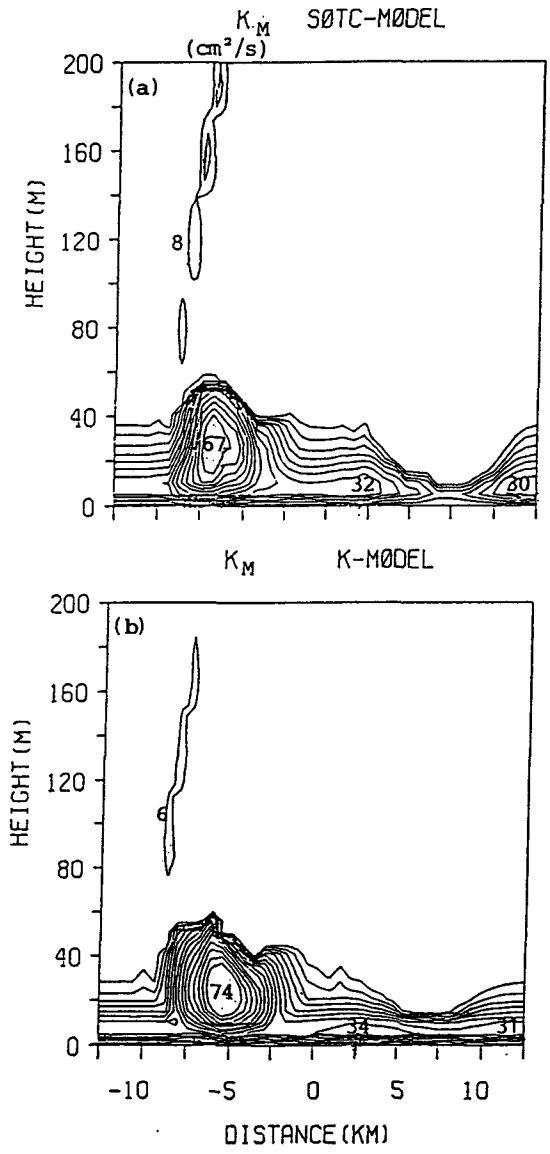

FIG. 3. As in Fig. 1, but for the vertical eddy diffusion coefficient, K_M.

layer properties in a benthic region of relatively complicated stratification and fine spatial structure and 2) to use the numerical experiments to study the dynamics of the BBL and its interaction with the CF. The model was checked against Ekman layer theory as well as against other BBL models (i.e., Weatherly and Martin 1978; Peggion and Weatherly 1990), and showed a good agreement for neutral and simple stratification cases. For the complicated structure associated with the CF and its interaction with the BBL, an analytical model or simultaneous fine measurements in the deep ocean seem to be unreachable at this time. Therefore, numerical models are essential tools in studying this region. Most of the observations that are presented as comparisons with the results of the model were reported by Weatherly and Kelley (1982, 1985a). Since the observations were taken at different periods and locations (within the HEBBLE area), and since temporal variabilities exist in this region, care must be taken making point-to-point comparisons. The main goal here is to compare qualitatively the various model results with observations.

With constant geostrophic forcing of $V_0 = -0.1$ m s^{-1}, the spinup time of the model was found to be about 2–4 days. After this period the inertial oscillations decay and the flow reaches a quasi-steady state in which the velocity field at each time step is adjusted to a slow change in the temperature field. We discuss here how the formation of the BBL changes the structure of the CF and how the CF affects the spatial structure of the BBL.

The bottom turbulence in the BBL changes the shape of the edges of the CF, as suggested by the simple linear model of Ezer and Weatherly (1989). However, significant differences can be seen in the present structure (e.g., Fig. 5) due to the additional effects of nonlinearity in the momentum equations, temperature advection, horizontal diffusion and thermal instability. The CF becomes less and less symmetric with time, due to different BBL dynamics in each edge. The initiation of

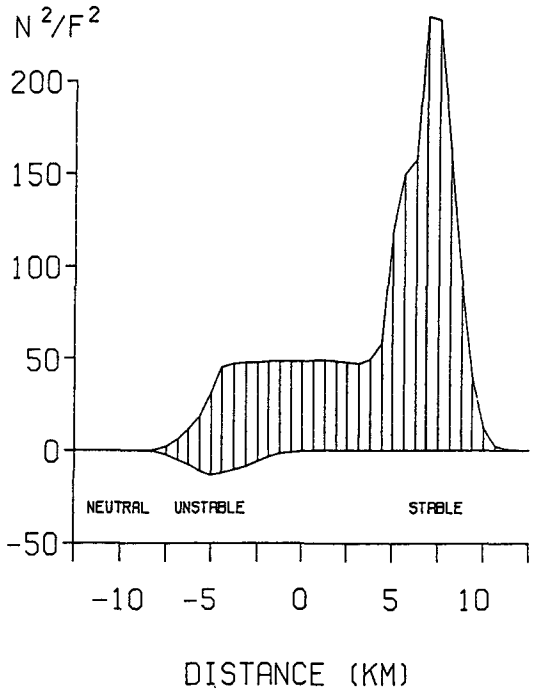

FIG. 4. The range of the stratification parameter N^2/f^2 (N is the Brunt–Väisälä frequency) across the CF after 4 days of simulation with the K-model. The initial value of N^2/f^2 on top of the BML was ~50. The stability of each region (as defined in section 1) is indicated.

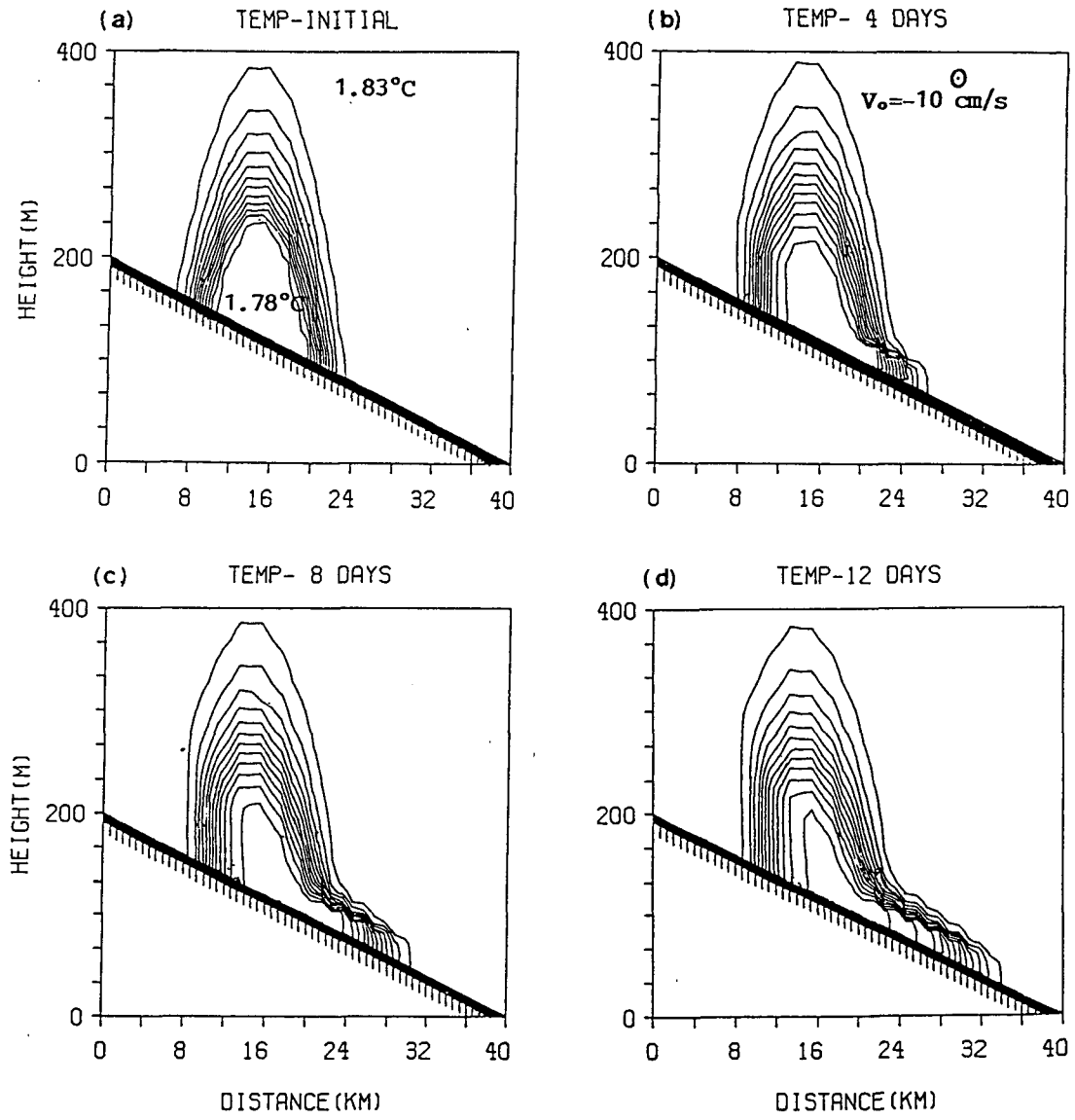

FIG. 5. The temperature structure of the CF on a sloping bottom calculated by the SOTC-model with constant forcing of $V_0 = -0.1$ m s^{-1}: (a) initial structure, (b) after 4 days, (c) after 8 days and (d) after 12 days. The potential temperature of the CF core and the interior are indicated in (a).

this change with time results from the Ekman veering in the BBL. Since the geostrophic velocity is southward, along the isobaths, in the BBL there is net flux to the left of the forcing velocity, i.e., eastward and downslope. In the downslope edge of the CF, advection of cold water from the core of the CF beneath warm interior water forms a thin BBL with very stable stratification. In the upslope edge, however, advection of warm interior water beneath cold water of the CF forms an unstable region with large thermal turbulence and thick BML (Figs. 3 and 5). Other regions of large eddy viscosity are in the center of the CF where the BML is comparably thick, and outside the CF where the stratification is almost neutral (Fig. 3). The two different mechanisms related to each edge confirm the results of Weatherly and Martin (1978), who found that if the Ekman flow is from cold to warm region (i.e., as the case in the downslope region) the BML cools with time while its thickness does not change much, but if the Ekman flow is from warm to cold region (i.e., as the case in the upslope region) the BML thickness increases with time while its temperature does not change much. The asymmetric structure of the CF produced by the model shows some similarities to observations (e.g., Fig. 6) where the spreading of cold layers downslope and the formation of very stable region there is

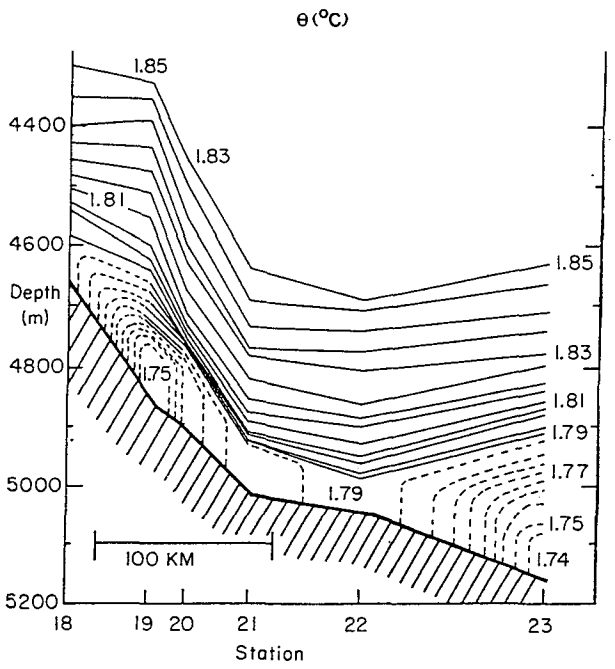

FIG. 6. An example of the temperature structure across the CF taken at about 40.5°N, 61°W in September, 1979 (from Weatherly and Kelley 1982). Note the large vertical temperature gradient in the downslope edge of the CF. Dashed segments represent those isotherms in which the location of their intersection with the bottom is unknown (i.e., between CTD sections).

also evident. The dual structure in Fig. 6, as well as cold eddies found elsewhere in the western North Atlantic (e.g., Ebbesmeyer et al. 1986) could be the result of cold water advected by the Ekman flow and eventually separated from its parent source (e.g., the CF), as suggested by Fig. 5.

b. *The spatial structure of the velocity field*

The along-isobath component of the flow relative to the geostrophic velocity of the interior (i.e., $v - V_0$) is shown in Fig. 2. In the upslope side of the CF $|v| < |V_0|$, while in the downslope side $|v| > |V_0|$ due to the thermal wind effect associated with the structure of the CF. The maximum difference $\approx 4 \times 10^{-2}$ m s^{-1}. This will also affect the characteristics of the BBL, since the friction velocity is now a function of x. Note that the larger portion of the CF has velocities greater than the interior (which agree with the finding of Ezer and Weatherly 1989); thus integrating over the CF cross-section would result in a southward net flow greater than the background flow, similar to the case of translation of cold eddies on a sloping bottom (Nof 1983).

Horizontal sections across the CF at different heights are shown in Fig. 7. The temperature cross section shows the frontal structure, which is very similar to the one reported by Weatherly and Kelley (1985). Spatial variations in the v component are associated with the thermal wind effect and are evident from the bottom up to the top of the CF core at about 100 m, while variations in the u component are associated with Ekman veering and are limited to the lower 15 m of the BBL. Note that the veering has maxima and minima at the downslope and the upslope edges respectively. The large velocity gradients (u_x and v_x) result in large vertical velocities (Fig. 11) and large horizontal diffusivity there.

c. *The temperature profiles*

Weatherly and Kelley (1982, 1985) show that vertical profiles taken across the CF can differ greatly in the BML thickness and in the temperature gradient in the transition layer. The temperature profiles that were chosen to demonstrate these differences and the associated velocity profiles represent the following different locations with respect to the CF (Fig. 8a):

1) a location out of the CF with homogeneous stratification for comparison with the stratified cases.
2) a location in the upslope front with unstable stratification.
3) a location in the upslope side of the CF where thermal wind effects oppose the interior velocity.
4) a location in the center of the CF where the BML thickness is maximum but with no thermal wind effects.
5) a location in the downslope side of the CF where thermal wind effects support the interior velocity.
6) a location farther downslope where cold water advected from the core forms a large temperature gradient in the base of the transition region.

The specific location of each of these profiles as well as the characteristics of the BBL at each location are summarized in Table 1. The temperature profiles calculated by the model (Fig. 8a) show good agreement with observations (Fig. 8b).

Special attention is now given to the existence of unstable profiles, which is quite a rare phenomenon for the benthic boundary layer. The unstable temperature profiles reported here, as well as those reported by Weatherly and Kelley (1985) are not restabilized by the salinity profiles. By comparison, unstable stratification is more common in the atmospheric boundary layer, but its cause, the upward heat flux across the earth's surface has a negligible effect in the oceanic boundary layer (Ezer and Weatherly 1989). The thermal stability to convective overturning of a fluid can be estimated by the Rayleigh number $\mathrm{Ra} = g\beta(\delta\theta)d^3/(K_M K_H)$, where d is the layer thickness, $\delta\theta$ the temperature difference and K_M and K_H represent average diffusivity values for the BBL. From the results of the model Ra $\approx$ 1200 (Weatherly and Kelley 1985, ap-

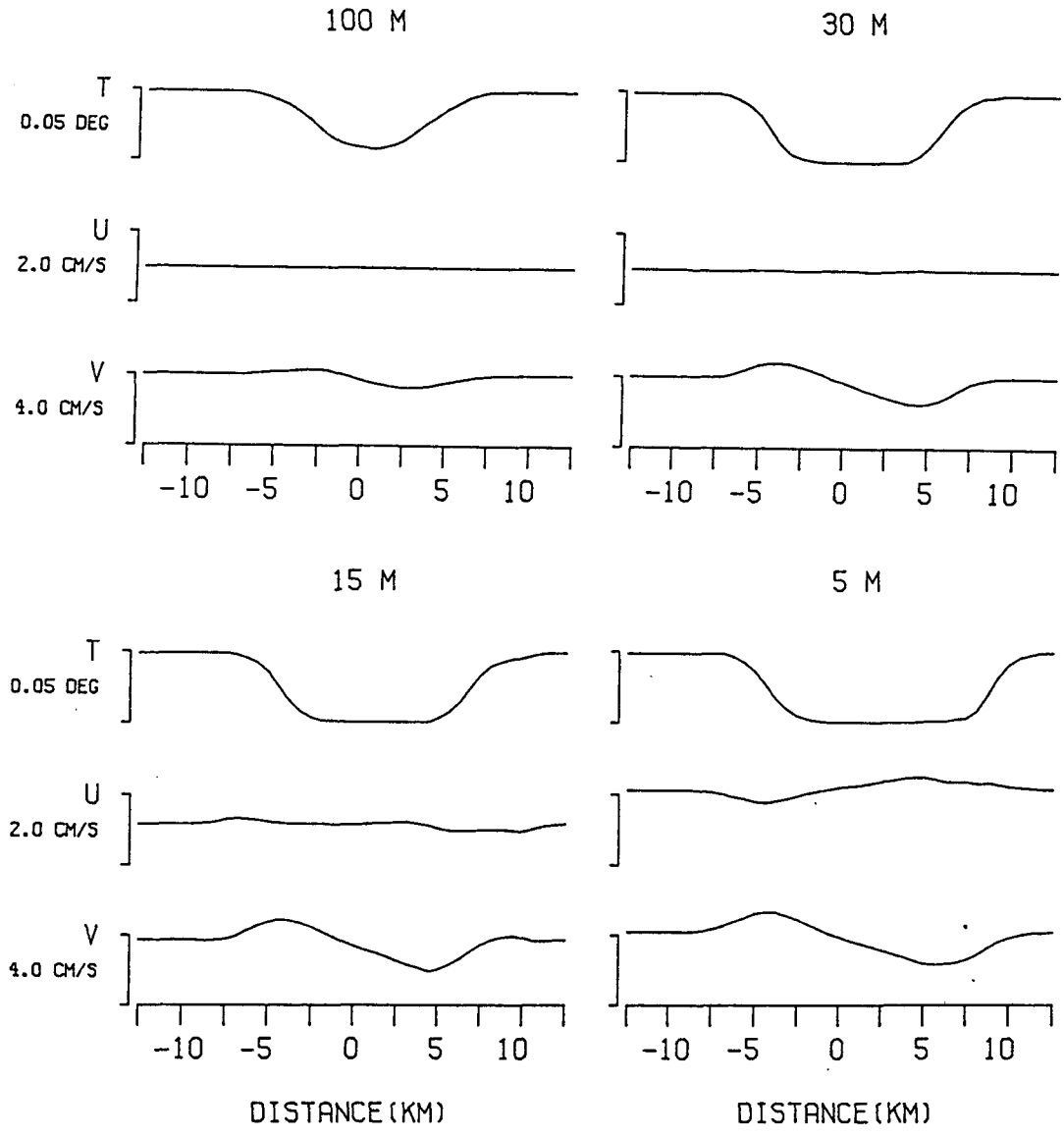

FIG. 7. Horizontal variations of temperature and velocity components across the CF at different levels above the bottom calculated by the SOTC-model after 4 days of integration.

proximated a similar value from the observations), which is comparable to the critical value $Ra_c = 1108$ (Turner 1973). Therefore, generation of convective motion near the upslope front of the CF seems plausible.

d. The velocity profiles and the Ekman spirals

The deviation of the velocity profiles from the "classical" Ekman profile (i.e., profile 1 in Fig. 9) are obvious. Other characteristics of the BBL such as the veering angle, the overshoot of the velocity and the eddy diffusivity are altered as well (Table 1). Moreover, the problem of identifying the BBL thickness solely from velocity profiles becomes apparent. The major factors responsible for these differences are the thickness and the stability of the BML, and the thermal wind effects in the transition region above the BML. Only in regions where the BML thickness is smaller than the BBL thickness of a homogeneous case (i.e., profiles 5 and 6), does the Ekman layer (inferred from the velocity profiles) occupy the whole BML. The thermal wind effect can be seen in the vertical gradient of the v component (Fig. 9b). It is also responsible for a change in the "overshoot" value (i.e., the maximum velocity is found in the BBL rather than in the interior). Compared to an overshoot $\approx 0.4 \times 10^{-2}$ m s^{-1} in the homogeneous case, the overshoot cannot be found in

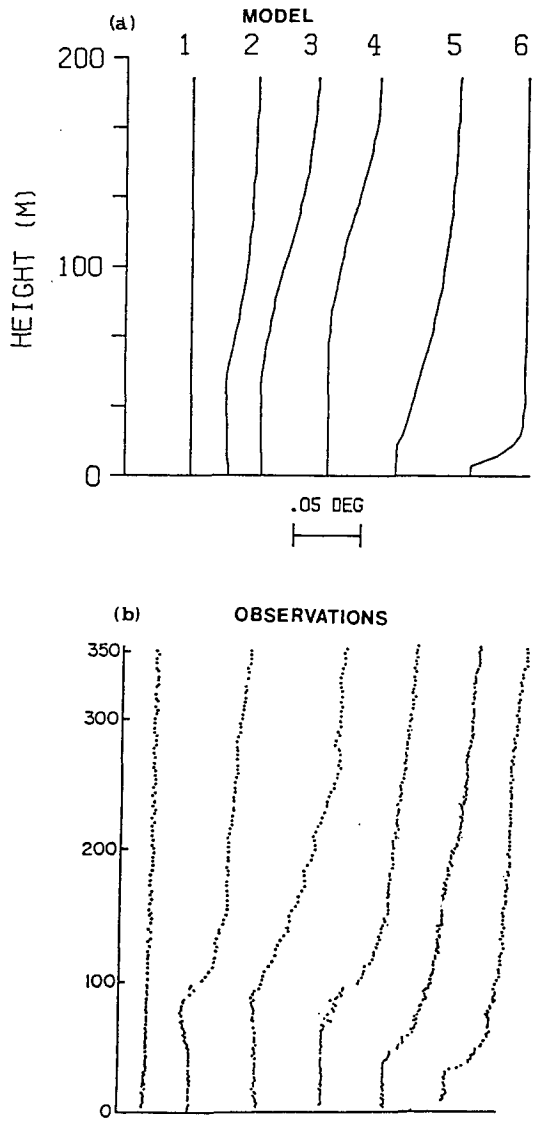

FIG. 8. Vertical temperature profiles: (a) Profiles calculated by the SOTC-model after 4 days of integration (see Table 1 for the location of each profile), (b) Example of profiles measured in the HEBBLE area at about 40.2°N, 62.5°W (from Weatherly and Kelley, 1985). The location of each measured profile with respect to the CF is approximated from the near-bottom temperature.

profile 2, but is as large as 2.3×10^{-2} m s^{-1} in profile 5 (Table 1). The larger overshoot of profile 4 compared to profile 1 indicates a "buoyant-slope" effect (see section 2) rather than thermal wind effect. The thermal wind effect and the resultant modification of the velocity profiles as indicated by the numerical calculations is evident in measurements taken in the vicinity of the CF (e.g., Fig. 10). The somewhat thicker BBL seen in the measured profiles (Fig. 10) compared to the model's result (Fig. 9b) may be due to larger velocity ($V_0 \approx 0.12$–0.15 m s^{-1} in the measurements compared to 0.1 m s^{-1} in the model). Deviation of velocity profiles associated with other effects such as nonlinearity and horizontal diffusion are considered later.

Ekman spirals, or the veering of the horizontal velocity vector in the BBL, are shown in Fig. 11. Deviations from the classical Ekman spiral are clear. Less veering is found in the upslope region (i.e., profiles 2 and 3) compared to the downslope region (i.e., profiles 5 and 6). For the friction parameter used here the veering angle between the direction of the forcing flow and the bottom stress changes between a minimum of about 8° in the upslope region to a maximum of about 12° in the downslope region, compared to 10° in neutral stratification (Table 1). The thermal wind effect can be also seen in the Ekman spirals, where the velocity vector decreases (e.g., profile 2 in Fig. 11) or increases (e.g., profile 5) before the Ekman veering starts.

e. The vertical circulation in the Cold Filament

A streamfunction to describe the circulation on an x–z plane is defined by $\Phi_x = w$ and $\Phi_z = -u$, and can be calculated from the velocity field by integrating $-u$ from the bottom to z, assuming $\Phi = 0$ on the bottom. The streamfunction shown in Fig. 12 represents the cross-stream circulation, i.e., the deviation from the southward geostrophic flow. Only very close to the bottom does the flow move downslope across the CF with little spatial variation. Otherwise, three counterclockwise circulation patterns can be seen (however, only the flow in the center forms a complete closed-circulation cell). In the upslope side of the CF, a water mass from the upper portion of the BBL convects when reaching the front and returns upslopeward at a higher level. In the downslope side of the CF, a water mass from the upper layers ($\sim$100 m above the BBL) is pumped into the BBL, and then advected downslope in the BBL. Near the core of the CF, a closed circulation is seen, centered around the place where $|v|$ is maximum. Water from the cold core is convected along the downslope side of the transition region and then pumped back into the core near the center.

Ekman pumping out of the BBL occurs near the fronts while pumping into the BBL occurs near the center (Fig. 12) as expected from the fact that the center is a region of high pressure (e.g., Pedlosky 1979). However, unlike the flow described by Pedlosky, the direction of the flow in the upslope region of the BBL is from low to high pressure, since it is driven by the geostrophic flow of the interior.

f. Transmissivity structure and detachment of bottom layers

Another unusual phenomenon observed in this region, which may be explained with the aid of the nu-

TABLE 1. The characteristics of the BBL at different regions of the modeled area (those of Fig. 8–10). The location of each profile is given with respect to the initial center of the CF.

	Profile					
	1	2	3	4	5	6
Location (km)	−10	−5	−2.5	0	+5	+8
Bottom temperature (°C)	1.828	1.817	1.785	1.780	1.781	1.787
BML thickness H (m)	—	~50	~60	~80	10	5
BBL thickness h (m)	39	44	39	34	10	5
Maximum K_M (cm^2 s^{-1})	31	60	32	30	21	15
Maximum u (cm s^{-1})	1.5	1.1	1.3	1.6	2.1	2.0
Overshoot ΔV (cm s^{-1})	0.4	—	—	0.6	2.3	1.2
Veering angle α (°)	10.0	7.9	9.4	10.4	11.6	11.7

merical experiments, is the vertical and horizontal structure of the near bottom transmissivity. Measuring the optical transmissivity per meter path length (in percent) of the water is one of the ways to study the transport of suspended sediments in bottom layers; small transmissivities correspond to relatively turbid water while large transmissivities correspond to relatively clear water. These measurements can be used to identify bodies of water or to study turbulent processes.

In the region near the CF, the thickness of the BML inferred from temperature and transmissivity profiles is usually quite similar (Weatherly and Kelley 1982). This is not unexpected, since the turbulence in the BBL mixes heat as well as suspended materials. However, layers homogeneous in turbidity and temperature were frequently found above the BML; sometimes they were more turbid than the BML. Weatherly and Kelley (1985), who first reported on this phenomenon in the HEBBLE region, suggested that the source of the water is detached bottom layers. They indicated that such separation of bottom layers is favored near the upslope front. Armi and D'Asaro (1980) reported detached bottom layers in another region of the benthic ocean as well.

The results of the model suggest two possible mechanisms for detachment of bottom layers. The thermal convection in the unstable region may be one mechanism of transporting suspended sediments from the bottom to the upper layers. Some of the overlying murkier layers reported in Weatherly and Kelley (1985) were found in the vicinity of the upslope front where unstable profiles were also measured. Vertical velocity produced by the convergency near the benthic fronts associated with the CF may be the second possible mechanism for detachment of bottom layers. Since the unstable region is found near the upslope front, both mechanisms appear likely to occur there. The vertical circulation pattern calculated by the model indicates that the core of the CF is the source of bottom layers separated near the downslope front while the

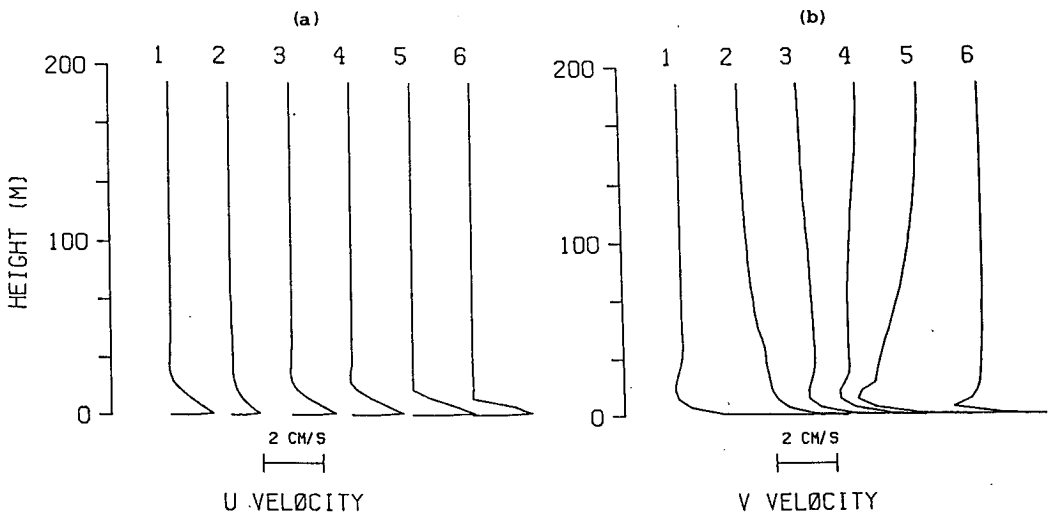

FIG. 9. Vertical velocity profiles after 4 days of integration with the SOTC-model: (a) Cross-stream velocity component u, (b) Along-stream velocity component v. The profiles are offset by 0.02 m s^{-1} with $(u, v) = (0, -0.1$ m s$^{-1})$ at 200 m.

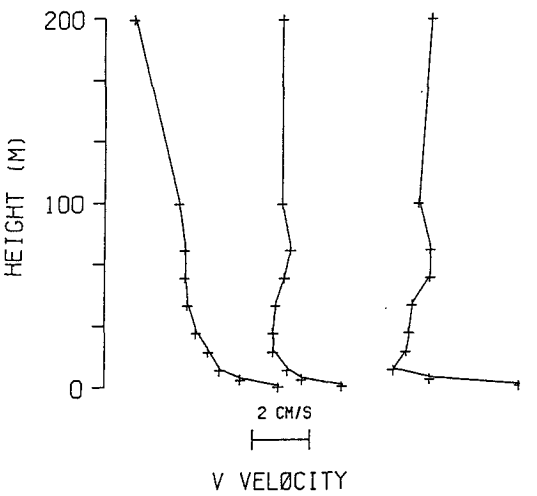

FIG. 10. An example of along-stream velocity profiles from the HEBBLE area at about 62.2°W, 40.2°N. They are from different periods during 1984 with similar interior velocity but with different location with respect to the CF. The location of each current meter is indicated by "+".

origin of the overlying water near the upslope front is bottom layers upslope of the CF. This could explain the observation of Weatherly and Kelley (1985) which indicated different types of water masses for the overlying layers. The vertical velocity near the fronts is as large as $w \approx 4 \times 10^{-5}$ m s^{-1} $\approx$ 3.5 m day^{-1} (compared to $w \approx 10^{-8}$ m s^{-1} outside the CF). Therefore, in a time scale of the order of a few inertial periods the whole BBL could be detached from the bottom.

Weatherly and Kelley (1985) also reported that the murkiest BML water is often found upslope of the CF core center (e.g., Fig. 13). This finding is consistent with the model's prediction that the maximum K_M is expected to be found upslope of the CF center (Fig. 3). Because of higher turbulence there, the suspended sediment should stay suspended longer and the water should be relatively murkier.

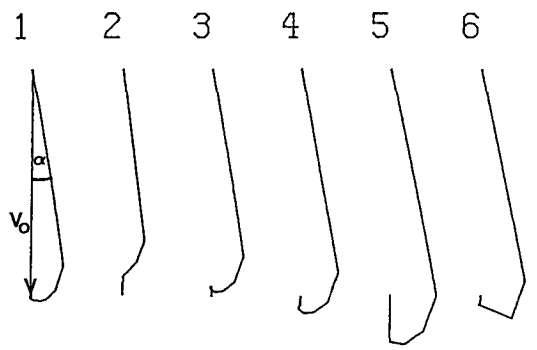

FIG. 11. Ekman spirals, i.e., velocity hodographs. The velocity vector in the interior V_0 and the veering angle α are indicated for profile 1. The location of each profile is the same as in Fig. 8a.

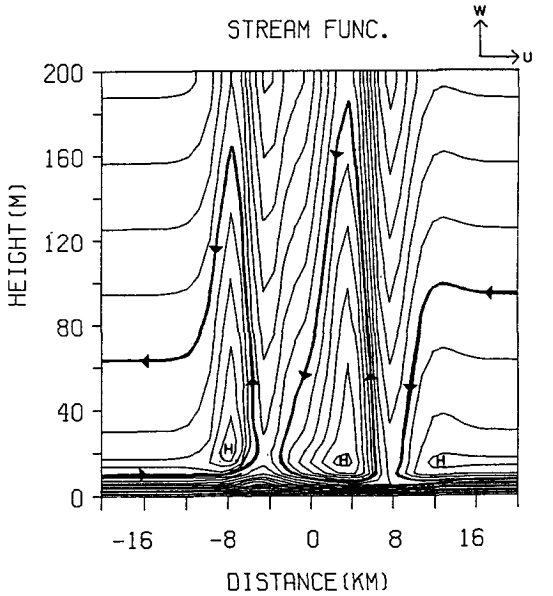

FIG. 12. Vertical streamfunction Φ associated with the cross-geostrophic flow (u and w components). The flow patterns in three circulation cells (those discussed in the text) are indicated. The contour interval is 6×10^{-3} m^2 s^{-1}, and the value of Φ varies between zero (on the bottom) and 0.1 m^2 s^{-1} (in the regions indicated by "H").

g. *Long term temperature changes in the CF*

The interaction between the BBL and the CF results in a significant change in the CF structure due to mixing

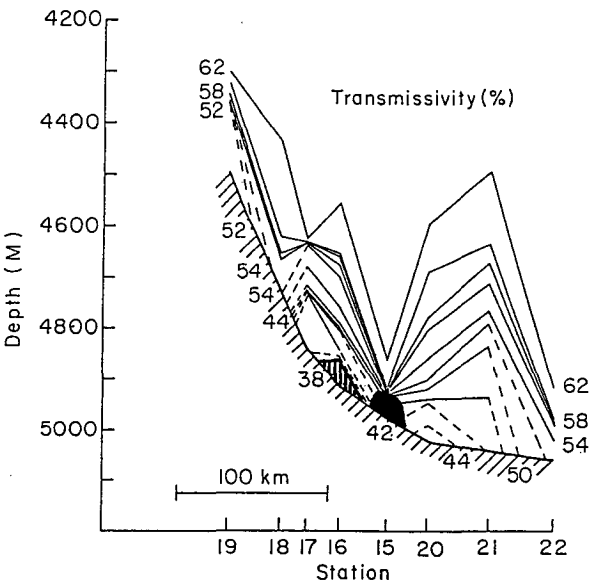

FIG. 13. Transmissivity transect from the HEBBLE area at about 40°N, 62.5°W taken in September 1980 (from Weatherly and Kelley 1982). Note that the murkiest region (i.e., the region of smallest transmissivity; the dashed area) is upslope to the CF core (the dark area).

and exchange of water between the CF and the interior. After the quasi-steady state is reached, the structure of the core of the CF does not change much, but its temperature increases slightly with time as a result of diffusion effects and intermixing with the interior. The model shows that the temperature of the core increases by about 3 m°C during a 30 day period with constant geostrophic forcing. With the two-dimensional assumptions of the model we can approximate variations in the y direction from variations with time. In 30 days the CF will move some 260 km; thus the rate of warming along its path is $D\theta/Dy \approx (12\ \text{m°C})/(1000\ \text{km})$. For comparison, Weatherly and Kelley (1985) found that the CF warms up by about 30 m°C between 56°30'W to 36°N which gives $D\theta/Dy \approx (15\ \text{m°C})/(1000\ \text{km})$. Although the primary intention of the present study is to investigate the short-term dynamics of the CF, further simulations (not presented here) seem to show that the CF is a relatively stable feature which keeps its identity for a period long enough to complete its pass along the continental rise, as observations suggested (Weatherly and Kelley 1985). In fact, the structure of the CF after these longer runs looks very similar to that shown at the end of the runs presented here. This is consistent with some other studies of Ekman layers in stratified fluids on inclined slopes, done in the laboratory (P. Rhines 1989, personal communication) and done numerically (Weatherly and Martin 1978), which indicate that after a few days Ekman transport downslope is nearly stoped by buoyancy forces, vertical recirculation, and dilution of the downslope edge.

4. Horizontal diffusion and nonlinear effects

Scaling analysis of the momentum equations indicates that the dominant terms in the x-momentum equation are the geostrophic component and the vertical diffusion (i.e., the classical Ekman balance in BBLs). However, in the y-momentum equation nonlinear and horizontal diffusion terms may become nonnegligible due to the two-dimensional nature of the flow. For the simulations described here, it was found that in the transition region above the BML the terms wv_z and $(A^y v_x)_x$ are of the same order of magnitude as the Coriolis term fu while uv_x term is at least one order of magnitude smaller (the scale analysis of each term in the primitive equation model is discussed in detail in Ezer 1989). However, do these effects significantly modify the velocity profiles and the characteristics of the BBL? To answer this question, the SOTC-model was used to calculate the velocity profiles as before, but this time all the nonlinear and the horizontal diffusion terms in the momentum equations were neglected. The results of this experiment are:

1) The characteristics of the BBL (the maximum u, the overshoot value and the veering angle; see table 1) do not change more than 3% by neglecting the nonlinear and the horizontal diffusion effects.

2) The profiles of the along-stream velocity component, v, are not modified significantly compared to the profiles calculated by the full primitive equation model (a typical change of about 1% in the v value in the BBL is found).

3) The changes in the profiles of the cross-stream velocity component, u, have the following typical order: 2% in the lower 5 m of the BBL, 1%–10% in the layers higher than 100 m, and 10%–100% in the transition region in-between. As expected, the largest modifications were found near the fronts.

These results show that the u component in the transition region is the most likely candidate to be affected by the nonlinearity and the horizontal diffusivity of this region. Nevertheless, in a practical point of view, in the region where the modification is significant, the magnitude of u is about 10^{-3} m s^{-1}, thus it is doubtful that observations could detect these effects. Although it seems that the BBL is not much affected by the nonlinearity and the horizontal diffusivity, the long term dynamics of the transition region, however, may be effected. One such effect that is noticed is the widening of the fronts due to horizontal diffusion and as a secondary result the vertical velocity changes significantly.

Further experiments (not reported here) indicate that reducing the forcing velocity V_0 or making the initial CF thinner would increase the relative importance of the nonlinear terms. However, here only the experiments with realistic conditions are reported.

5. Summary and conclusions

In previous studies of the near-bottom deep layers in the western North Atlantic, spatial structures were attributed to the Gulf Stream meanders and eddies (e.g., Hendry 1985; Kelley and Weatherly 1985). These variations were also studied with numerical models (e.g., Peggion and Weatherly 1989; Richards 1984). However, while these studies considered only the mesoscale range ($\geq$50 km), the present study discussed variations in the range of the local internal Rossby radius of deformation ($\leq$5 km). Since the latter small-scale variations cannot be detected by the more easily available surface measurements, it is important to note that they exist. Such small-scale variations are often neglected in deep ocean studies.

A new eddy viscosity scheme for numerical models was presented. It includes the use of the recent formulas suggested by Ezer and Weatherly (1989), together with a new formulation for unstable cases. The produced eddy diffusion coefficients fit the ones calculated by the more complicated SOTC-model while saving a significant amount of calculations. It is found that in cases of unstable stratifications, additional thermal turbulence must be added to the K-model in order to give

realistic results. In the new formulations for the unstable case, the eddy diffusion coefficients depend only on a length scale and on the local stratification.

A primitive equation numerical model with second-order turbulence closure scheme (based on the level 2½ scheme of Mellor and Yamada 1974, 1982) was used to study the interaction between the BBL and the CF under constant forcing condition. The results of the model compared favorably with observations obtained in the HEBBLE area. It was found that the cross-isotherm BBL flow that results from the Ekman veering in the boundary layer was the major source of the modification of the CF structure. With constant southward geostrophic forcing (i.e., along isobaths as the case for the CF) the Ekman transport in the BBL was eastward (i.e., downslope). As a result, in the downslope region of the CF the intrusion of cold core water under warm interior water formed a very thin and stable BBL, while in the upslope edge of the CF the intrusion of warm interior bottom water into the core formed an unstable, thermally convective, region characterized by large thermal turbulence. The horizontal and the vertical scales of the downslope cold tongue depend mainly on the Ekman veering and on the depth of the Ekman layer, respectively. This asymmetry effect increased with time: the downslope BBL cooled down while keeping its depth unchanged and the upslope BBL increased its depth while keeping its temperature almost unchanged. A similar phenomenon has been suggested by the results of the one-dimensional BBL model of Weatherly and Martin (1978); however, the two-dimensional model discussed here allowed us to study the mechanism and the implications of this dynamics in more detail. The result of the interaction was a quasi-steady state in which a steady velocity field was adjusted to a slow change of the temperature field. The adjustment of the velocity field was on time scales of the order of the inertial period (about a day), while the time scale for the changes of the temperature was somewhat larger (order of tens of days). The asymmetry effect due to Ekman veering may apply not only to a CF-like feature, but to cold eddies as well. Laboratory experiments of cold eddies drifting on a sloping bottom indicate a downslope intrusion very similar to the one reported here (Mory et al. 1987). Further applications of this study could be drawn even for the dynamics of fronts in the upper ocean. Cushman-Roisin (1981), for example, indicated a similar asymmetric effect in the structure of the upper ocean mixed layer near a frontal region. the upper-ocean front, associated with convergence of Ekman transports, is affected by similar dynamic processes as the ones affecting the benthic fronts discussed here. In the upper-ocean case, however, the wind-stress curl plays the same role as the thermal wind effect in the near-bottom case studied here.

In light of the numerical simulations, some of the previously unaccounted characteristics of the BBL in this region could be explained. Weatherly and Kelley (1985), for example, reported on the existence of unstable temperature profiles in the vicinity of the CF which could not be stabilized by the salinity profiles. The current study showed that such profiles were formed near the upslope edge of the CF due to the Ekman veering described before. The Rayleigh number for this region was near critical, suggesting that instantaneous thermal convection was possible. However, as long as the geostrophic forcing persisted, the continuous cross-isotherm BBL flow kept the unstable region from totally homogenizing even though the eddy diffusion there was very large.

Another unusual phenomenon of this area was the detachment of bottom layers reported by Weatherly and Kelley (1985). These layers, which were found mostly upslope of the center of the CF, were characterized by turbid water (indicated by small optical transmissivity). These observations were consistent with the results of the model, which showed that the largest turbulence was found upslope of the center of the CF, near the upslope front, where the stratification was unstable. The large turbulence in this region allowed the suspended sediments to stay suspended longer (and thus the water was expected to be murkier there). Moreover, the model indicated that large vertical velocity upward was also found near this front. Therefore, a mechanism of detachment of bottom layers and of maintaining their turbidity were favored in the upslope region.

Considering the two types of BMLs in the deep ocean reported by Amos et al. (1971), the present study suggested two new formation mechanisms of BMLs in boundary layers of the second type (i.e., those of anomalous cold water). These two mechanisms are associated with the interaction between such cold water masses and the BBL. The first mechanism is thermal turbulence mixing (i.e., as in the upslope region), which is often neglected in oceanic BBLs, but lead here to appreciable thickening of the BML. However, unlike the atmospheric BBL where the source of the turbulence is the heat flux across the bottom, its oceanic source is cross-isotherm bottom flow. The second mechanism is the near bottom Ekman transport of cold water masses (i.e., as in the downslope region) which may eventually separate from their parent source. Both mechanisms may be important in a region with anomalous water mass and energetic forcing.

Another goal of the study was to indicate the small-scale spatial variations of the BBL, and to understand the modified velocity profiles that were observed in the HEBBLE region. The most important factor affecting these variations were found to be the thermal wind effect that is related to inclined benthic fronts. It changed the friction velocity, the Ekman veering in the BBL, and as a result the velocity profiles in the CF were much different from those obtained by classical Ekman dynamics.

Other effects that may modify the dynamics of the BBL are nonlinearity and horizontal diffusivity, which are often neglected in studies of benthic regions but may be important in frontal regions such as the one discussed here. Although it seems that they are much less important than the thermal wind effects in modifying the characteristics of the BBL, their main effect is on the long-term dynamics of the transition and the frontal regions. If one is interested only in producing reasonable near bottom velocity profiles, the study showed that the major parameters that should not be neglected are temperature advection and thermal wind effects. For long-term studies of transition regions and benthic fronts the nonlinear and the horizontal diffusivity effects should also be considered. In any case, the study showed that small scale spatial variations in the characteristics of the BBL are expected across the CF. This study also suggests comparable variations are not unlikely across deep, cold lenses similar to those reported by Ebbesmeyer et al. (1986).

Three-dimensional CF simulation with realistic, variable forcing in space and time are currently being undertaken.

Acknowledgments. Dr. David Dietrich is thanked for his contribution in developing the numerical schemes of the model. This research was supported by the Office of Naval Research through Contracts N00014-82-C-0404 and N00014-87-J-0115 and by Sandia National Laboratory through Contract 09-7900. The U.S. Department of Energy supported part of the numerical modeling through a grant to the Supercomputer Computational Research Institute. One of us (TE) was partially supported by Israel Oceanographic and Limnological Research Ltd., The National Institute of Oceanography.

REFERENCES

Amos, A. F., L. Gordon and E. D. Scheider, 1971: Water masses and circulation patterns in the region of the Blake-Bahama Outer Ridge. *Deep-Sea Res.*, **18,** 145–166.

Armi, L., and E. D'Asaro, 1980: Flow structures of the benthic ocean. *J. Geophys. Res.*, **85,** 469–484.

Arya, S. P. S., 1973: Neutral planetary boundary layer above a non-homogeneous surface. *Geophys. Fluid Dyn.*, **4,** 333–355.

Boning, C. W., 1988: Characteristics of particle dispersion in the North Atlantic: An alternative interpretation of SOFAR floats results. *Deep-Sea Res.*, **35,** 1379–1385.

Businger, J. A., and S. P. S. Arya, 1974: Height of the mixed layer in the stably stratified planetary boundary layer. *Advances in Geophysics,* Vol. 18A, Academic Press, 407–418.

Cushman-Roisin, B., 1981: Effects of horizontal advection on upper ocean mixing: A case of frontogenesis. *J. Phys. Oceanogr.*, **11,** 1345–1356.

Dietrich, D. E., M. G. Marietta and P. J. Roache, 1987: An ocean modeling system with turbulent boundary layers and topography: Numerical description. *Int. J. Num. Methods Fluids,* **7,** 833–855.

Ebbesmeyer, C. C., B. A. Taft, J. C. McWilliams, C. Y. Shen, S. C. Riser and H. T. Rossby, 1986: Detection, structure, and origin of extreme anomalies in a Western Atlantic oceanographic section. *J. Phys. Oceanogr.*, **16,** 591–612.

Ezer, T., 1989: A study of the Benthic Boundary Layer associated with the Cold Filament of the western North Atlantic. Ph.D. Dissertation, Florida State University, 98 pp.

——, and G. L. Weatherly, 1990: Small-scale spatial structure and long-term variability of near bottom layers in the HEBBLE area. *Deep-Sea Res.*, in press.

——, and ——, 1989: On eddy diffusion profiles in oceanic bottom boundary layers associated with cold eddies and filaments. *Bound.-Layer Meteor.*, **48,** 83–97.

Griffiths, R. W., P. D. Killworth and M. E. Stern, 1982: Ageostropic instability of ocean currents. *J. Fluid Mech.*, **117,** 343–377.

Gross, T. F., A. J. Williams and W. D. Grant, 1986: Long term in-situ calculations of kinetic energy and Reynolds stress in a deep sea boundary layer. *J. Geophys. Res.*, **91,** 8461–8469.

Hendry, R. M., 1985: Deep circulation south of the Gulf Stream at 50°W. *Progress in Oceanography,* Vol. 14, Pergamon, 191–207.

Kelley, E. A., G. L. Weatherly and J. C. Evans, 1982: Correlation between surface Gulf Stream and bottom flow near 5000 meter depth. *J. Phys. Oceanogr.*, **12,** 1150–1153.

——, and ——, 1985: Abyssal eddies near the Gulf Stream. *J. Geophys. Res.*, **90,** 3151–3159.

McLean, S. R., and J. Yean, 1987: Velocity and stress in the deep-ocean boundary layer. *J. Phys. Oceanogr.*, **17,** 1356–1365.

Mellor, G. L., and T. Yamada, 1974: A hierarchy of turbulence closure models for planetary boundary layers. *J. Atmos. Sci.*, **31,** 1791–1806.

——, and ——, 1982: Development of a turbulence closure model for geophysical fluid problems. *Rev. Geophys. Space Phys.*, **20,** 851–875.

Mofjeld, H. O., and J. W. Lavelle, 1984: Setting the length scale in a second order closure model of the unstratified bottom boundary layer. *J. Phys. Oceanogr.*, **14,** 833–839.

Mory, M., M. E. Stern and R. W. Griffiths, 1987: Coherent baroclinic eddies on a sloping bottom. *J. Fluid Mech.*, **183,** 45–62.

Munk, W. H., 1966: Abyssal recipes. *Deep-Sea Res.*, **13,** 707–730.

Nof, D., 1983: The translation of isolated cold eddies on a sloping bottom. *Deep-Sea Res.*, **30,** 171–182.

——, 1984: Oscillatory drift of deep cold eddies. *Deep-Sea Res.*, **31,** 1395–1414.

Pedlosky, J., 1979: *Geophysical Fluid Dynamics,* Springer-Verlag, 624 pp.

Peggion, G., and G. L. Weatherly, 1990: On the interaction of the bottom boundary layer and deep rings. *Deep-Sea Res.*, in press.

Priestly, C. H. B., 1959: *Turbulent Transfer in the Lower Atmosphere.* University of Chicago Press, 130 pp.

Richards, K. J., 1982: Modeling the benthic boundary layer. *J. Phys. Oceanogr.*, **12,** 428–439.

——, 1984: The interaction between the bottom mixed layer and mesoscale motions of the ocean: A numerical study. *J. Phys. Oceanogr.*, **14,** 754–768.

Smith, P. C., 1975: A streamtube model for bottom boundary current in the ocean. *Deep-Sea Res.*, **22,** 853–873.

Tennekes, H., and J. J. Lumley, 1972: *A First Course in Turbulence.* The MIT Press, 300 pp.

Turner, J. S., 1973: *Buoyancy Effects in Fluids.* Cambridge University Press, 357 pp.

Weatherly, G. L., and P. J. Martin, 1978: On the structure and dynamics of the oceanic bottom boundary layer. *J. Phys. Oceanogr.*, **8,** 557–570.

——, and E. A. Kelley, 1982: "Too cold" bottom layers at the base of the Scotian Rise. *J. Mar. Res.*, **40,** 985–1012.

——, and ——, 1985: Two views of the Cold Filament. *J. Phys. Oceanogr.*, **15,** 68–81.

Yamada, T., 1975: The critical Richardson number and the ratio of the eddy transport coefficients obtained from a turbulence closure model. *J. Atmos. Sci.*, **32,** 926–933.

——, 1979: An application of a three dimensional simplified second order closure numerical model to study atmospheric effects of a large cooling pond. *J. Atmos. Environ.*, **13,** 693–704.